工程科学学报
Chinese Journal of Engineering

钢/Ar及钢/渣界面非金属夹杂物碰撞团聚行为原位观察

吴明晖 程礼梅 任英 张立峰

***In situ* observation of collision and agglomeration behavior of non-metallic inclusions at steel/Ar and steel/slag interfaces**

WU Minghui, CHENG Limei, REN Ying, ZHANG Lifeng

引用本文:
吴明晖, 程礼梅, 任英, 张立峰. 钢/Ar及钢/渣界面非金属夹杂物碰撞团聚行为原位观察[J]. 北科大：工程科学学报, 2025, 47(4): 727–738. doi: 10.13374/j.issn2095–9389.2024.11.01.001
WU Minghui, CHENG Limei, REN Ying, ZHANG Lifeng. *In situ* observation of collision and agglomeration behavior of non–metallic inclusions at steel/Ar and steel/slag interfaces[J]. *Chinese Journal of Engineering*, 2025, 47(4): 727–738. doi: 10.13374/j.issn2095–9389.2024.11.01.001

在线阅读 View online: https://doi.org/10.13374/j.issn2095–9389.2024.11.01.001

工程科学学报，第 47 卷，第 4 期：727−738，2025 年 4 月
Chinese Journal of Engineering, Vol. 47, No. 4: 727−738, April 2025
https://doi.org/10.13374/j.issn2095-9389.2024.11.01.001; http://cje.ustb.edu.cn

钢/Ar 及钢/渣界面非金属夹杂物碰撞团聚行为原位观察

吴明晖[1)]，程礼梅[2)]，任　英[1)✉]，张立峰[3)✉]

1) 北京科技大学冶金与生态工程学院，北京 100083　2) 攀钢集团研究院有限公司特钢所，成都 610031　3) 北方工业大学机械与材料工程学院，北京 100144
✉通信作者，任英，E-mail: yingren@ustb.edu.cn；张立峰，E-mail: zhanglifeng@ncut.edu.cn

摘　要　首先介绍了高温共聚焦扫描显微镜（HT-CSLM）的工作原理及主要功能，详细介绍汇总了近年来使用高温共聚焦显微镜对钢中夹杂物团聚的研究进展，包括对钢液表面、钢渣界面及渣表面夹杂物碰撞、团聚、长大的原位观察，动力学研究及模型推导. 探讨了当前计算夹杂物之间吸引力的毛细力模型，分析了密度、尺寸、距离等因素对钢中夹杂物团聚碰撞趋势的影响大小，并为后期高温共聚焦显微镜在夹杂物碰撞的研究方向提供思路.

关键词　高温共聚焦激光扫描显微镜；钢液界面；夹杂物；团聚碰撞；毛细力模型
分类号　TF4

In situ observation of collision and agglomeration behavior of non-metallic inclusions at steel/Ar and steel/slag interfaces

WU Minghui[1)], *CHENG Limei*[2)], *REN Ying*[1)✉], *ZHANG Lifeng*[3)✉]

1) School of Metallurgical and Ecological Engineering, Beijing University of Science and Technology, Beijing 100083, China
2) Pangang Group Research Institute Co., Ltd., Chengdu 610031, China
3) School of Mechanical and Materials Engineering, North China University of Technology, Beijing 100144, China
✉Corresponding author, REN Ying, E-mail: yingren@ustb.edu.cn; ZHANG Lifeng, E-mail: zhanglifeng@ncut.edu.cn

ABSTRACT　The working principle and the main functions of the high-temperature confocal scanning laser microscope (HT-CSLM) are presented. *In situ* observation of the evolution of high-temperature microstructure of materials can be performed using the HT-CSLM. This is important for studying in detail the processes of material melting, solidification, high-temperature stretching, martensitic transformation, etc. It can also be used in the metallurgical field to study the dissolution, collision, agglomeration, and growth behavior of inclusions. The recent advancements in the aggregation of inclusions using the HT-CSLM are summarized. *In-situ* observations of collisions, aggregation, and growth of inclusions on the surface of molten steel, slag, and at the steel–slag interface, along with the dynamic studies and model derivations, are included. The collision behavior of non-metallic inclusions at the steel/Ar interface has been analyzed using high-temperature confocal microscopy. This is an important parameter for understanding the collision, agglomeration, and growth behavior of non-metallic inclusions in steel and for exploring the methods to improve steel cleanliness. According to the law of agglomeration of inclusions at the steel/Ar interface, inclusions with similar phases exhibit attraction: the attraction between the solid phases is the strongest, followed by that of the semisolid–semisolid pairs and the liquid–liquid pairs. For inclusions with different states, both attractive and repulsive forces exist simultaneously. The difference between the forces depends on their physical properties, in particular, the contact angle between inclusions and molten steel. Research on the parameters of the capillary force model shows that the

收稿日期：2024−11−01
基金项目：国家重点研发计划资助项目（2023YFB3709900）；国家自然科学基金资助项目（U22A20171）；中国宝武低碳冶金创新基金资助项目（BWLCF202315）；攀钢–北科大钒钛研究院科研资助项目

effect of the density, size, and contact angle of inclusions is significant on capillary suction, while that of the steel surface tension is relatively weaker. Previous studies have included Al_2O_3, Al_2O_3–SiO_2, Al_2O_3–CaO, MgO, Al_2O_3–MgO, Al_2O_3–Ce_2O_3, and Ca–, Si–, and Al-type inclusions in carbon steel. However, there has been limited research on other types of composite inclusions, such as Ti-type oxides and titanium aluminum spinel. The influence of different gradients of the same element on the collision between inclusions should also be taken into consideration. The current model for calculating the attractive force between inclusions is explored, and the impact of factors such as density, size, and distance on the trend of inclusion aggregation and collision in steel is analyzed. The scope for further research on the use of high-temperature confocal microscopy in the field of inclusion collision is also included. The K–P model for calculating the capillary force between inclusions at the steel/Ar interface still has many limitations: a large amount of physical property data, such as the contact angles between various inclusions and the molten steel, is required. This in turn makes the calculation of the magnitude of capillary forces between all inclusions on the surface of the molten steel difficult. Therefore, correcting the K–P model or establishing a new collision model for inclusions on the surface of molten steel is crucial in the study of the collision trend of inclusions on the surface of molten steel.

KEY WORDS　high temperature confocal laser scanning microscope; surface of molten steel; inclusions; collision; model of capillary force

随着工业水平的快速提高，钢的洁净度对于需要满足更高机械性能要求的优质钢材愈发重要. 钢中非金属夹杂物是影响钢洁净度的重要因素，了解并控制钢中非金属夹杂物的碰撞、团聚与长大行为对提高钢洁净度非常重要[1−2]. 利用高温共聚焦扫描激光显微镜（HT-CSLM）可在高温下对钢液表面进行原位观察[3]，目前已广泛应用于夹杂物的碰撞和团聚现象研究，Yin 等[4−5] 使用高温共聚焦观察了氧化铝夹杂物在钢/Ar 表面的碰撞行为. 近年来，国内外学者使用 CSLM 对钢/Ar 及钢/渣界面非金属夹杂物碰撞团聚行为进行了大量研究[6−15]. 本文基于以上研究阐述 CSLM 研究非金属夹杂物碰撞团聚的常用研究方法及夹杂物碰撞模型，并总结了各类非金属夹杂物碰撞团聚的行为及影响因素.

1　研究方法及研究现状

HT-CSLM 由日本 Lasertec 公司研发，将共聚焦激光扫描、红外加热、拉伸等先进技术结合，可以原位观察材料高温组织的演化，是直观研究材料熔化、凝固、高温拉伸、马氏体相变等过程的重要工具，在冶金领域也可用于研究夹杂物的溶解、碰撞、团聚与长大行为[16−21]. HT-CSLM 由高温加热炉和激光共聚焦显微镜两大部分组成，工作原理如图 1 所示. 激光共聚焦显微镜采用紫色激光器扫描照明成像，扫描速度可达 120 帧每秒. 在高温下对样品进行原位观察时，高温加热炉中的卤素光源红外反射集光，在热电偶附近形成 ϕ10 mm×10 mm 的圆柱形超高温加热空间，对放置在热电偶上方的坩埚及坩埚内的样品进行加热，升温速率最快可达到 300 ℃·s^{-1}; 炉身连接的真空装置及 Ar 气进气装置可使炉内处于真空或惰性气氛，真空度可达 10^{-2} Pa; 加热炉的冷却装置包括水冷系统及 He 气急冷系统，最大冷却速率可达 100 ℃·s^{-1}.

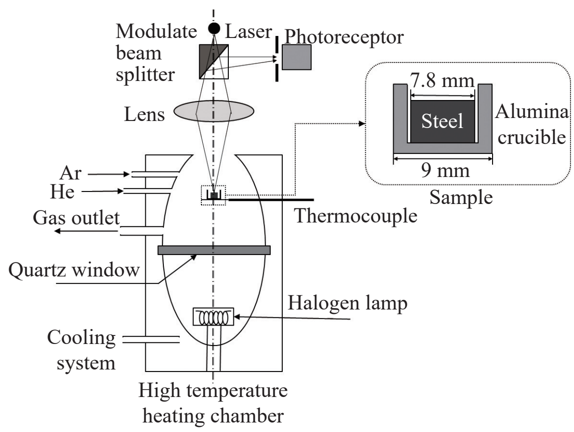

图 1　高温共聚焦原理图[22]

Fig.1　High-temperature confocal principle diagram[22]

CSLM 研究夹杂物碰撞团聚行为的实验装置如图 1 虚线部分所示，将装有钢样或钢渣样品的坩埚放置在热电偶上并进行加热，在高温下观察不同界面夹杂物的碰撞团聚行为.

近年来国内外学者对非金属夹杂物碰撞团聚行为的研究很多，所研究夹杂物包括 Al_2O_3[4−5,23]，80%Al_2O_3–20%SiO_2[5,24]、 MgO[25]、 93%Al_2O_3–7%MgO[25−26]、Al_2O_3–CaO–SiO_2[27]、不同比例 Ca/Al 的 Al_2O_3–CaO[5,28−31]、复合夹杂物 CaO–MgO–Al_2O_3[27]、CaO–MgO–Al_2O_3–SiO_2[16,24]、Al_2O_3–Ce_2O_3[32−33]、Ce_2O_2S[34]、SiO_2[35]、TiN[36−38]、MnS[39−40]、Ti_2O_3[41] 等，夹杂物前数字代表其质量分数，所研究界面主要集中在钢/渣界面[16,20,28−30,42]、钢/Ar 界面[4−5,20,25,42−46]、固/

液界面[26,28,47]及渣表面[29]. 表 1 总结了应用 CSLM 观察夹杂物碰撞的相关文献[4−5,20,23−29,32−34, 36,39,44,47−49]. 其中 CaO 缩写为 C, Al_2O_3 缩写为 A, SiO_2 缩写为 S, MgO 缩写为 M, 缩写字母后的数字表示每种夹杂物的平均含量, 例如, CA60S 代表 xCaO–60%Al_2O_3–$y$$SiO_2$.

根据 CSLM 拍摄的夹杂物碰撞图像, 通过公式 (1) ~ (5) 可以得到一个客体夹杂物向一个停滞的主体夹杂物移动时所受到的吸引力, 此外, 如果两夹杂物体积大小相互接近, 可以通过公式 (6) 对吸引力进行修正, 两夹杂物碰撞过程如图 2[33,43] 所示, 将夹杂物等效为球体, 在某些文献中将夹杂物等效为圆盘状[5].

$$v_1 = (d_3 - d_2)/\Delta t \tag{1}$$

$$v_2 = (d_2 - d_1)/\Delta t \tag{2}$$

$$a_1 = (v_2 - v_1)/\Delta t \tag{3}$$

$$m_2 = (4/3)\pi \left(R_2^*\right)^3 \times \rho \tag{4}$$

$$F = a_1 \times m_2 \tag{5}$$

$$F = a_1 \times m_1 \times m_2/(m_1 + m_2) \tag{6}$$

式中: Δt 是两次测量之间的时间步长, s; d_1, d_2, 与 d_3 分别是两个夹杂物在碰撞前Δt、$2\Delta t$ 与 $3\Delta t$ 时的距离, m; v_1 与 v_2 分别是碰撞前两个步长间断夹杂物的平均速度, $m\cdot s^{-1}$; a_1 是夹杂物的加速度, $m\cdot s^{-2}$; m_1、m_2 分别是两个夹杂物的质量, kg; R_1^*、R_2^*分别是两个夹杂物的等效半径, m; ρ 是夹杂物的密度, $kg\cdot m^{-3}$; F 是两个夹杂物之间的吸引力, N.

由于文献中研究的夹杂物颗粒主要是 Al_2O_3 及包含 Al_2O_3 的复合夹杂物, 但在实际生产过程中, 除了 Al_2O_3 及包含 Al_2O_3 的复合夹杂物外, 还包括 MnS、TiN、MgO 等夹杂物及少部分稀土化合物, 但目前这些夹杂物研究较少.

2 钢/渣界面夹杂物碰撞

钢/渣界面的夹杂物团聚碰撞的情况更为复杂, 当两夹杂物间距小于 100 ~ 150 μm 时, 存在长距离吸引力和排斥力[28]. 如图 3 所示. 钢/渣界面处的夹杂物可能会被渣流强制凝聚. 钢/渣界面处不同夹杂物凝聚的距离范围不同, 但当前工作未对此做出解释. 这个问题值得在今后的工作中深入研究.

除了钢/Ar 界面与钢/渣界面, Wikström 等[28−29]还通过实验发现液态 Al_2O_3–CaO 夹杂物在钢渣界面上不会发生团聚, 但对已经转移到渣中的液态 Al_2O_3–CaO 夹杂物的实验表明, 夹杂物的团聚能力显著提高, 其原因可能是, 在渣表面的夹杂物之间的自由能高于钢/渣界面上的夹杂物之间的自由能, 但并未考虑夹杂物溶解在渣中的情况, 因此在今后的工作中, 可以考虑结合液态渣中夹杂物团聚和溶解进行更系统的观察实验.

3 钢/Ar 界面夹杂物碰撞

3.1 钢/Ar 界面夹杂物碰撞研究现状

根据状态的不同, 可将夹杂物分为固态、半固态和液态夹杂物. 对于钢/Ar 界面夹杂物的团聚碰撞行为, Shibata 等[52]通过实验发现固态夹杂物如 Al_2O_3 之间存在着明显的吸引力, 因此发生团聚碰撞的趋势更高, 半固态夹杂物如 Al_2O_3–CaO–SiO_2 复合夹杂物有着类似的规律, 而纯液态夹杂物如 CaO–Al_2O_3 之间的相互吸引力相对不明显, 发生团聚碰撞的趋势也较小, 如图 4 所示. 此外, 文献还提出了吸引力作用范围这一概念, 并报道 Al_2O_3 对之间的吸引力作用范围为 50 μm, 而 80% Al_2O_3–20% SiO_2 对之间的吸引力作用范围为 40 μm, 吸引力大小均在 10^{-16} ~ 10^{-14} N.

随后, Kimura 等[25], Nakajima 和 Mizoguchi[27]通过对 16Cr Al–Si 脱氧不锈钢及 16Cr Si 脱氧不锈钢表面夹杂物的碰撞团聚观察发现, 同样状态的夹杂物颗粒之间存在着吸引力, 如固–固、半固–半固、液–液以及固–半固, 但不同状态的夹杂物颗粒之间吸引力很小, 甚至存在着排斥力, 如固–液夹杂物, 这一结论与 Yin 等[4]的报道结果相似但不完全一致. 此外, Nakajima 等[27]还发现, 93%Al_2O_3–7%MgO 夹杂物对与 MgO 夹杂物对之间的吸引力大小相近, 均在 5×10^{-18} ~ 5×10^{-16} N, 约为 Al_2O_3 及 80%Al_2O_3–20%SiO_2 夹杂物对之间吸引力的 1/20; 而 93%Al_2O_3–7%MgO 对与 MgO 对之间的吸引力作用范围为约为 22 μm, 远小于 Al_2O_3 及 80%Al_2O_3–20%SiO_2 夹杂物对. 因此该文献认为, 在钢/Ar 界面, 固态夹杂物更容易团聚碰撞形成较大团簇, 对于具有不同状态的夹杂物对的情况, 吸引力和排斥力都存在, 差异取决于物理性质, 特别是夹杂物与钢液的接触角.

Vantilt 等[42]通过观察 Mn–Si 脱氧钢钢液表面固态 Al_2O_3 夹杂物、固态 Al_2O_3–MnO 夹杂物及液态 Al_2O_3–MnO–SiO_2 夹杂物的碰撞团聚行为, 发现固态夹杂物可自由移动形成团簇, 液态夹杂物被迫团聚, 这与文献 [25,27] 的研究相似; Coletti 等[16]

表 1 CSLM 研究非金属夹杂物碰撞

Table 1 CSLM study on the collision of non-metallic inclusions

	Author	Year	Types of steel/slag	Composition of inclusions	Inclusion size/μm	Collision or not	Capillary force/attractive force/N	Cause of collision	References
Steel/Ar interface	Yin et al	1997	Low carbon aluminum killed steel	Al_2O_3	10	Yes	10^{-16}	Capillary force	[4−5]
			Low carbon aluminum killed steel	Al_2O_3	2	Yes	—	Capillary force	[4]
			Fe–3%Si	A80S	1–3	Yes	7.0×10^{-16}	Capillary force	[4−5]
			HSLA	CA60S	5–10	No			[4]
			Si-killed	CA80S	1–3	Yes	4.0×10^{-16}	Capillary force	[4]
			Si-killed	CAS95	5–10	Yes	8.2×10^{-15}	Capillary force	[4]
			Si-killed	CA50S	5–10	No	—	—	[4]
			High-sulfur free cutting steel	CA80	3–5	Yes	6.5×10^{-14}	Capillary force	[4]
			High-sulfur free cutting steel	CA60	5–10	Yes	10^{-16}	Capillary force	[4]
			High-sulfur free cutting steel	CA50	5–10	No			[4]
	Kimura et al	2000 2001	Low carbon aluminum-magnesium killed steel	AM50	5.32	Yes	5.0×10^{-18}–5.0×10^{-16}	Capillary force	[25−26]
	Kimura et al	2001	Low carbon aluminum-magnesium killed steel	MgO	—	—	—	—	[25]
	Nakajima et al	2001	16Cr stainless steel	C30A60M10	1.5–15.5	Yes	10^{-14}–10^{-17}	Capillary force	[27]
	Nakajima et al	2001	16Cr stainless steel	C40A55M5	<40	No			[27]
	Vantilt et al	2004	Silicon manganese treated steel	Al_2O_3-MnO-SiO_2	10	No			[42]
	Wikstrom et al	2008	Calcium treated steel	CA50	10–80	Yes	10^{-13}–10^{-15}	Capillary force	[29]
	Appelber g et al	2008	Fe–20%Cr	Ce_2O_3	20	Yes	—	—	[32]
	Shao et al	2011	High-sulfur free cutting steel	MnS	40	No			[39]
	Kang et al	2011		CA50		No			[48]
	Bin and Bo	2012	16Mn	Ce_2O_2S	<5	No			[34]
	Jiang et al	2014	Low oxygen special steel	CaO–MgO–Al_2O_3–SiO_2	5	Yes		Capillary force	[47]
	Mu et al	2017 2018		TiN		Yes		Capillary force	[20,44]

表 1 (续)

Table 1 (Continued)

	Author	Year	Types of steel/slag	Composition of inclusions	Inclusion size/μm	Collision or not	Capillary force/attractive force/N	Cause of collision	References
	Tian et al	2018	GCr15	TiN	10	Yes		Cavity bridge force(CBF)	[36]
	Mu and Xuan	2019		TiO_x–Al_2O_3	10–20	Yes		Capillary force	[50]
	Wang and Liu	2020	Al-killed	Al_2O_3	15–30	Yes	10^{-15}–3.0×10^{-14}	$F=\frac{m_1\times m_2\times a_1}{(m_1+m_2)}$	[33]
				Ce–Al–O	10–30	Yes	1.3×10^{-16}–2.0×10^{-14}		[33]
				Ce_2O_3	10–30	Yes	1.3×10^{-16}–2.0×10^{-14}		[33]
				Ce–O–S	5–20	Yes	2.1×10^{-18}–6.0×10^{-16}		[33]
		2021		Ce_2O_3–SiO_2	5–20	Yes	4.3×10^{-17}–4.2×10^{-15}		[35]
				SiO_2	5–20	Yes	6.3×10^{-19}–1.2×10^{-16}		[35]
	Wu et al	2023	GCr15	MgO	5–20	Yes	10^{-17}–10^{-15}		[22]
	Wu et al	2024	304 stainless steel	La_2O_3–La_2S_3	5–20	Yes	10^{-18}–10^{-16}		[51]
Steel/slag interface	Misra et al	2000	50%CaO–50%Al_2O_3	Al_2O_3	5	Yes	10^{-16}–3.0×10^{-15}	When the slag is saturated with Al_2O_3 or the dissolution rate of Al_2O_3 is low, Al_2O_3 may agglomerate at the slag metal interface	[38]
	Misra et al	2001	CaO–Al_2O_3–MgO–SiO_2	TiN	5	Yes		TiN will agglomerate due to fluid flow	[37]
	Lee et al	2001	50%CaO–50%Al_2O_3	Al_2O_3		Yes			[30]
	Coletti et al	2003	Calcium treated steel	CA50	3–4	Yes		Hydrodynamic forces	[16]
	Vantilt et al	2004	CaO–Al_2O_3–MgO–SiO_2	Al_2O_3–MnO–SiO_2		No	—	Inclusions agglomerate at the slag/steel interface but do not collide	[42]
	Wikstrom et al	2008	Steel/slag interface	CA50		Yes			[28–29]
	Michelic et al	2015	CaO–Al_2O_3–MgO–SiO_2	Al_2O_3 Al_2O_3–MgO		No	—	—	[19]
	Mu et al	2016	Aluminum-magnesium	MgO	6	No	—	If there is no saturated MgO slag present, MgO inclusions disappear and no longer appear at 1873 K	[49]
Surface of slag	Wikström et al	2008		CA50		Yes			[28]

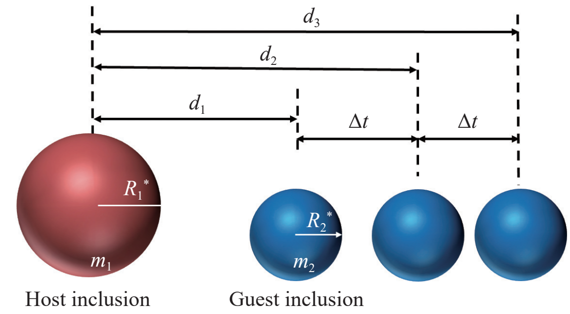

图 2　夹杂物碰撞过程[5,33,43]

Fig.2　Collision process of inclusions[5,33,43]

通过对 Ca 处理 Al 脱氧钢表面液态 $CaO–Al_2O_3$ 进行原位观察，得到了相同的结论. 梁高飞等[24] 观察了 $CaO–MgO–Al_2O_3–SiO_2$ 复合氧化物在 $AlSi_3O_4$ 不锈钢熔融表面的聚集行为，Appelberg 等[32] 报道了 $Ce_2O_3–Al_2O_3$ 夹杂物在 Fe–20% Cr 不锈钢钢液表面的团聚行为，根据钢中 [Ce]/[Al] 比例的不同，Appelberg 等人观察到了钢中不同类型的 $Ce_2O_3–Al_2O_3$ 夹杂物，但所有类型的夹杂物都可以碰撞团聚形成半径为 20 μm 左右的夹杂物簇. Wikström 等[29] 对高碳 Ca 处理 Al 脱氧钢钢/Ar 界面的两种 $CaO–Al_2O_3$ 夹杂物进行了原位观察，分别是液态的 50% CaO–50% Al_2O_3（CA50）夹杂物及半液态的 38%CaO–62%Al_2O_3（C38A62）夹杂物，发现半液体的 C38A62 夹杂物对之间碰撞是“自由”的，而液态的 CA50 夹杂物对之间碰撞是“自由”与“强制”的，这与以往的研究结论相似[16,27–28,42]. 同时 Wikström 等还声称当温度升高时，受钢液流动的影响，液态夹杂物可能“强制”在钢液表面发生碰撞团聚. Wang 和 Liu[33] 报道了 Al 脱氧钢/Ar 界面四种不同夹杂物对（Al_2O_3，

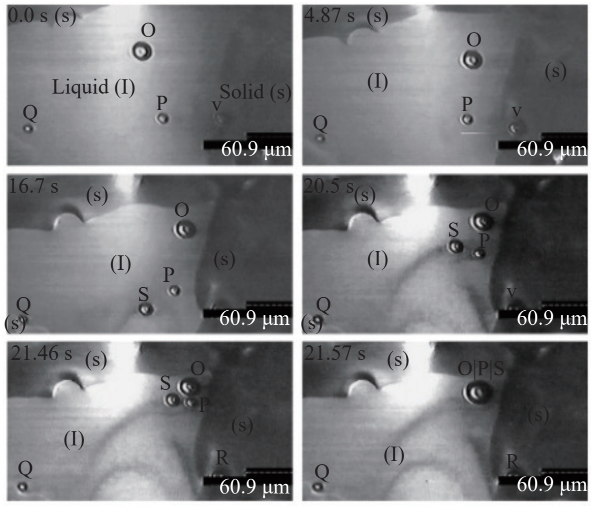

(a)

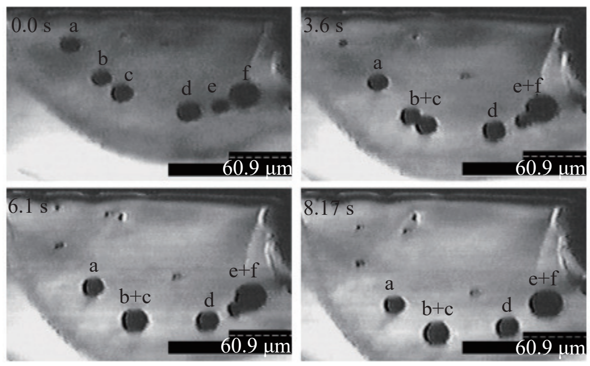

(b)

图 3　夹杂物在钢渣界面及渣表面团聚碰撞原位观察[28]. (a) 钢渣界面夹杂物的团聚碰撞现象; (b) 渣表面夹杂物的团聚碰撞现象

Fig.3　*In situ* observation of agglomeration and collision of inclusions at the interface and the surface of steel slag[28]: (a) agglomeration and collision phenomenon of inclusions at the interface of steel slag; (b) agglomeration and collision phenomenon of inclusions on the surface of slag

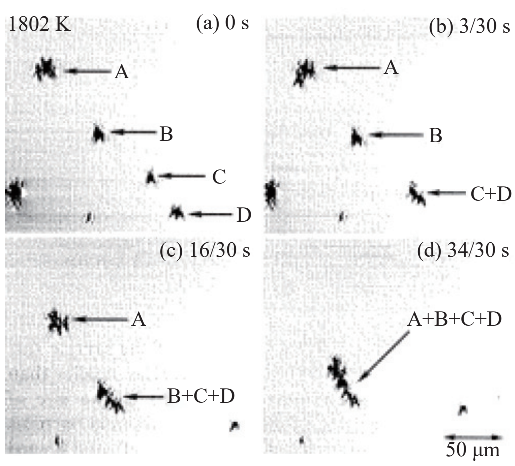

(a)

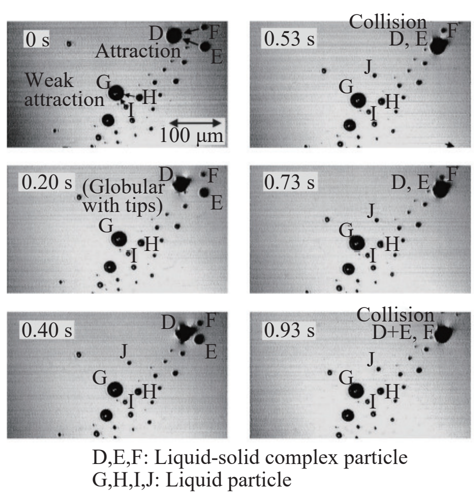

(b)

图 4　钢液表面夹杂物运动状态. (a) 固体 Al_2O_3 夹杂物碰撞[5]; (b) 液态夹杂物及半液态夹杂物运动状态[27]

Fig.4　Movement of inclusions on the surface of molten steel: (a) collision of solid Al_2O_3 inclusions[5]; (b) movement status of liquid inclusions and liquid–solid inclusions[27]

Ce–Al–O, Ce_2O_3, Ce–O–S) 之间吸引力大小为 Al_2O_3>Ce–Al–O>Ce_2O_3>Ce–O–S, 而 Ce–Al–O 与 Ce_2O_3 夹杂物对之间虽然吸引力较弱, 但仍能发生碰撞并团聚为更大的簇.

以往研究对不同的夹杂物在钢/Ar 界面的团聚碰撞行为结论大多相似, 但对 MgO–Al_2O_3 夹杂物在钢/Ar 界面的碰撞行为结论并不完全一致, Kang 等[48] 报道了 Al_2O_3 的碰撞团聚行为, 但没有发现 MgO–Al_2O_3 尖晶石夹杂物有任何的吸引或团聚的趋势; Du[53] 等人报道了 Fe–0.4C–1.0Si–0.3Mn–5.0Cr–1.2Mo–0.9V–Al 脱氧钢不添加 Mg 及添加 Mg 时钢/Ar 界面 Al_2O_3 夹杂物与 MgO-Al_2O_3 尖晶石的碰撞行为, Du 等虽然观察到了半径达 60 μm 的 MgO–Al_2O_3 尖晶石簇, 但数量与尺寸要远远小于 Al_2O_3 簇, 即 MgO–Al_2O_3 尖晶石碰撞趋势小于 Al_2O_3 夹杂物. 目前为止, 不同学者报道的 MgO–Al_2O_3 尖晶石夹杂物的团聚行为均不完全一致, 这可能与各钢种的不同物理性质或 MgO–Al_2O_3 尖晶石本身数量密度的不同有关.

现有研究普遍认为夹杂物之间的碰撞团聚趋势是由于碰撞界面上固体颗粒之间存在远距离吸引力, 而远距离吸引力是由毛细作用引起的. 图 5 为不同夹杂物对之间吸引力随距离的变化[5,25–27,33,35,43], 可知在钢液表面不同夹杂物的毛细吸力顺序为 Al_2O_3>$TiAlO_x$–Al_2O_3>Ce_2O_3>Ce–Al–O>Al_2O_3–SiO_2>Ce–O–S>Al_2O_3–Ca O>SiO_2>MgO>$MgAl_2O_4$, 这也与夹杂物在纯铁液面的接触角大小顺序基本一致[54], 而随着钢种的不同, 夹杂物接触角发生变化, 夹杂物在钢液表面的毛细吸力大小也会发生变化.

3.2 毛细吸力模型

前文已阐述夹杂物之间的碰撞团聚趋势是由于钢液表面固体颗粒之间存在远距离吸引力, 而远距离吸引力是由毛细作用引起的, 固体颗粒与钢液之间的接触角, 粒径和密度以及钢液的表面张力都会在不同程度上影响毛细管吸引力, 其中接触角影响较为强烈, 因此建立夹杂物碰撞毛细吸力模型对理解夹杂物碰撞有着重要意义, 如图 6[26] 为两个球形颗粒周围毛细管弯月面示意图.

1993 年, Paunov 等[57], 以及 Kralchevsky 和 Nagayama[58] 从理论上推导出了球形粒子 1 和 2 之间的毛细管力 F_C 和互相作用能ΔW方程, 如下式(7)和(8):

$$F_C=\frac{d(\Delta W)}{dL} \quad (7)$$

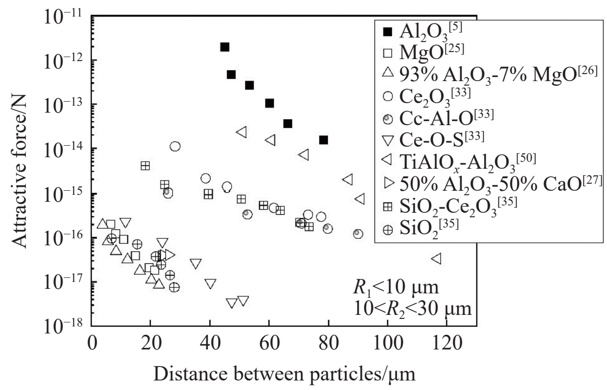

图 5 不同夹杂物对之间吸引力随距离的变化[5,25–27,33,35,50]

Fig.5 The variation of attractive force between different inclusions with distance[5,25–27,33,35,50]

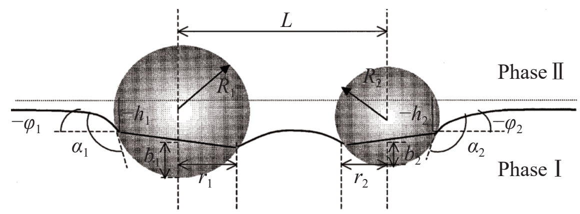

图 6 两个球形颗粒周围毛细管弯月面示意图[26,55–56]

Fig.6 Schematic of capillary meniscus around two spherical particles[26,55–56]

$$\Delta W=-\pi\gamma\sum_{k=1}^{2}\left(Q_k h_k-Q_{k\infty}h_{k\infty}\right)\left(1+O\left(q^2R_k^2\right)\right)R_k \quad (8)$$

式中: L 为两颗粒距离, m; ΔW 为毛细管相互作用能, J; q 为毛细管长度, m^{-1}; γ 为钢液表面张力, $J\cdot m^{-2}$; Q_k 和 $Q_{k\infty}$为两颗粒距离 L 和无穷大时的有效毛细管电荷; h_k 和 $h_{k\infty}$为两颗粒距离 L 和无穷大时的弯月面高度差, m; R_k 为夹杂物粒子半径, m; $O(x)$ 是该近似值的零函数.

q、Q_k 与 h_k 由式(9)、(10)和(11)得到:

$$q=\sqrt{\frac{(\rho_{\text{I}}-\rho_{\text{II}})g}{\gamma}}\approx\sqrt{\frac{\rho_{\text{I}}g}{\gamma}},\ \rho_{\text{I}}\gg\rho_{\text{II}} \quad (9)$$

$$Q_k=\frac{1}{2}q^2\left(b_k^2\left(R_k-\frac{1}{3}b_k\right)-\frac{4}{3}D_kR_k^3-r_k^3h_k\right) \quad (10)$$

$$\begin{aligned}h_k=&\left(\tau_k+2\ln\left(1-\exp\left(-2\tau_k\right)\right)\right)-\\&\left(Q_1+Q_2\right)\ln\left(\gamma_e qe\right)+\\&\left(Q_1-Q_2\right)\left(A-(-1)^k\sum_{n=1}^{\infty}\frac{2}{n}\frac{\exp\left(-n\tau_k\right)\sinh n\tau_k}{\sinh n\left(\tau_1+\tau_2\right)}\right)\end{aligned} \quad (11)$$

式中: ρ_{I} 为钢液密度, 7000 $kg\cdot m^{-3}$; ρ_{II} 为空气密度, 忽略不计; γ 为钢液表面张力, $N\cdot m^{-1}$; b_k 为颗粒浸没深度, m; D_k 为密度比; r_k 为毛细管弯月面半径, m; γ_e=1.78; g 为重力加速度, 9.8 $m\cdot s^{-2}$; A、τ_k、e 等参数是为简化方程设立的.

A、τ_k、e、D_k、b_k 及 r_k 的计算方程如下式（12）~（18）：

$$A=\sum_{n=1}^{\infty}\frac{1}{n}\frac{\sinh n(\tau_1-\tau_2)}{\sinh(\tau_1+\tau_2)} \tag{12}$$

$$\tau_k=\ln\left(\frac{b}{r_k}+\left(\frac{b}{r_k}+1\right)^{0.5}\right) \tag{13}$$

$$e^2=\left(L^2-(r_1+r_2)^2\right)\left(L^2-(r_1-r_2)^2\right)/(2L)^2 \tag{14}$$

$$D_k=(\rho_k-\rho_{\mathrm{II}})/(\rho_{\mathrm{I}}-\rho_{\mathrm{II}}) \tag{15}$$

$$b_k=R_k(1+\cos(\alpha_k+\varphi_k)) \tag{16}$$

$$\varphi_k=\arcsin(Q_k/r_k) \tag{17}$$

$$r_k=0.5\left(R_k\sin\alpha_k+\left(R_k^2\sin^2\alpha_k+4Q_kR_k\cos\alpha_k\right)^{1/2}\right) \tag{18}$$

式中：ρ_k 为夹杂物密度，$kg\cdot m^{-3}$；φ_k 为弯月面斜率；α_k 为夹杂物与钢液面接触角.

当两个夹杂物成分与大小相同时，公式（11）可被简化为公式（19）：

$$h_k'=Q_k(\tau_k+2\ln(1-\exp(-2\tau_k)))-(Q_1+Q_2)\ln(\gamma_e qe) \tag{19}$$

$$Q_{k\infty}=\frac{1}{6}q^2R_k^3\left(2-4D_k+3\cos\alpha_k-\cos^3\alpha_k\right) \tag{20}$$

$$h_{k\infty}=r_{k\infty}\sin\alpha_k\varphi_{k\infty}\frac{4}{\gamma_e q(1+\cos\varphi_{k\infty})} \tag{21}$$

Mu 等[44] 对公式做了最终简化，得到式（22）和（23）两个毛细力 F_C 的计算公式：

$$F_C=2\pi\gamma\frac{Q_1Q_2}{L}\left(r_k\ll L\ll q^{-1}\right) \tag{22}$$

$$F_C=\frac{2\pi\gamma Q_1Q_2\left(1-q^2L^2\right)}{L}(r_k\ll L) \tag{23}$$

与利用已发表文献中各夹杂物碰撞过程中吸引力对模型计算的毛细力结果进行对比，结果如图 7 所示.

3.3　非金属夹杂物在钢/Ar 界面团聚碰撞影响因素

3.3.1　夹杂物密度与尺寸对毛细吸力的影响

根据毛细吸力模型[43−44] 计算不同密度不同尺寸夹杂物之间毛细吸力大小，如图 8、图 9 所示. 研究表明，夹杂物的密度尺寸与毛细力成正相关的关系，当其他条件不变时，夹杂物密度与尺寸越大，夹杂物在钢液表面的毛细力越大. 图 10 为高温共聚焦对钢液表面观察的 $MgO\cdot Al_2O_3$ 夹杂物对之间随距离变化吸引力及模型计算得到的毛细力的变化趋势，实验计算结果与模型计算结果较为拟合.

在前人已有的研究基础上，本文作者通过观察不同 Mg 含量轴承钢表面夹杂物的碰撞现象，发现在轴承钢液表面夹杂物吸引力大小为 Al_2O_3> Al_2O_3–MgO> MgO，并且随着 Mg 含量的增加，夹杂物的碰撞趋势逐渐降低，因此关于 $MgO–Al_2O_3$ 尖晶石在钢/Ar 界面的碰撞行为还有待更深入的

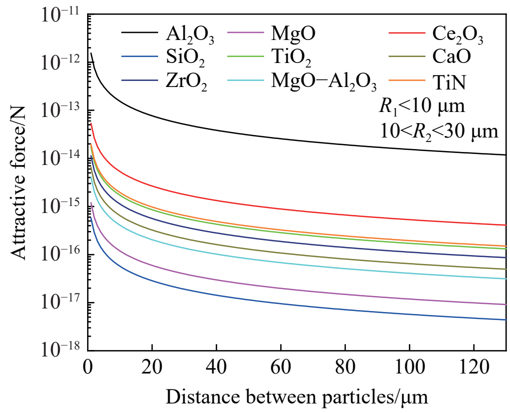

图 7　钢液表面不同夹杂物之间吸引力与毛细力的对比

Fig.7　Comparison of attractive and capillary forces between different inclusions on the surface of molten steel

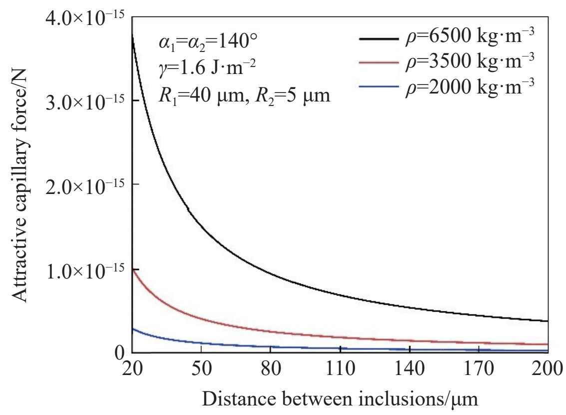

图 8　不同密度夹杂物间毛细吸力随距离的变化[44]

Fig.8　The variation of capillary suction force between inclusions of different densities with distance[44]

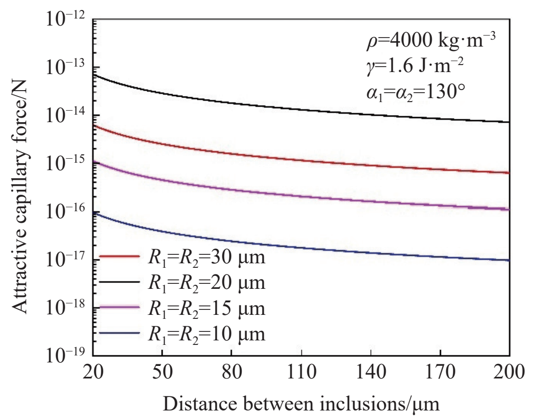

图 9　不同尺寸夹杂物间毛细吸力随距离的变化[43]

Fig.9　The variation of capillary suction force between inclusions of different sizes with distance[43]

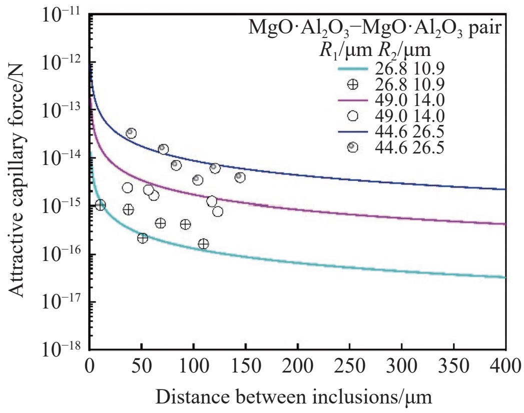

图 10 不同尺寸 MgO–Al$_2$O$_3$ 夹杂物碰撞过程中随距离变化吸引力[22,51]及毛细力的变化

Fig.10 Changes in attractive and capillary forces with distance during the collision of MgO–Al$_2$O$_3$ inclusions of different sizes[22,51]

研究; 另外研究了不同 La 含量 304 不锈钢表面夹杂物的碰撞现象, 发现随着 La 含量的增加, 夹杂物的碰撞趋势逐渐降低, 如图 11 所示; 一系列研究表明 Mg 与 La 的加入都会降低钢中夹杂物的碰撞趋势, 降低钢中夹杂物尺寸、生产高洁净钢有着显著效果.

3.3.2 接触角对毛细吸力的影响

接触角对吸引毛细管力的影响如图 12 所示, 该计算考虑了具有相同半径和相同密度的夹杂物, 值得注意的是, 当接触角为 90°时, 毛细力非常接近零, 而当接触角均大于或小于 90°时, 接触角越远离 90°, 毛细吸力越大. 实际上, Paunov 等[57]提出, 可以根据原始模型进行近似简化的计算, 简化公式见式(24), 根据公式可推导当接触角为 90°时, 弯月面恰好是水平的, 因此毛细力为零.

$$F = \frac{\mathrm{d}(\Delta W)}{\mathrm{d}L} \approx 2\pi\gamma \frac{r_1 r_2 \sin\varphi_1 \sin\varphi_2}{L} \qquad (24)$$

式中: φ_1、φ_2为弯月面斜率, °; r_1、r_2为毛细管弯月面半径, m.

3.3.3 钢液表面张力对毛细吸力的影响

钢液表面张力对毛细吸力的影响如图 13 所示[43], 随着表面张力从 1.9 J·m^{-2} 降到 1.1 J·m^{-2}, 毛细吸力

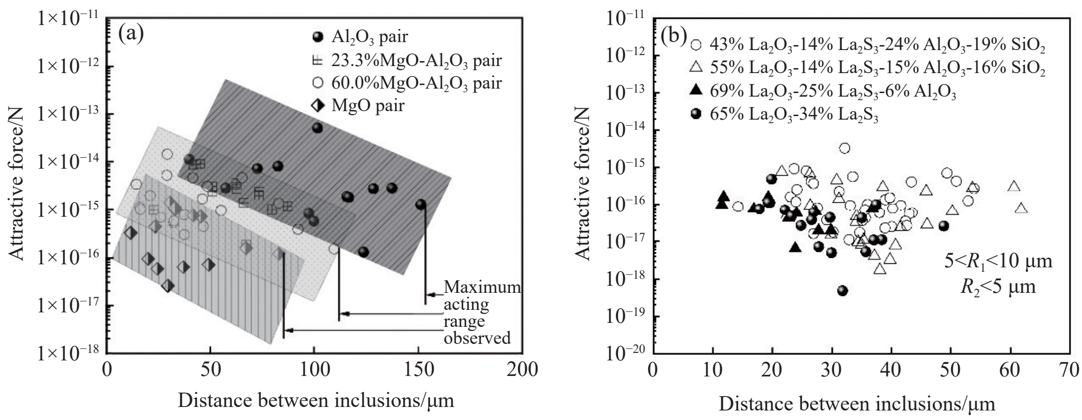

图 11 钢液表面不同含量夹杂物之间吸引力对比. (a) 含 Mg 夹杂物[22]; (b) 含 La 夹杂物[51]

Fig.11 Attractive forces between inclusions with different contents: (a) Mg inclusions[22]; (b) La inclusions[51]

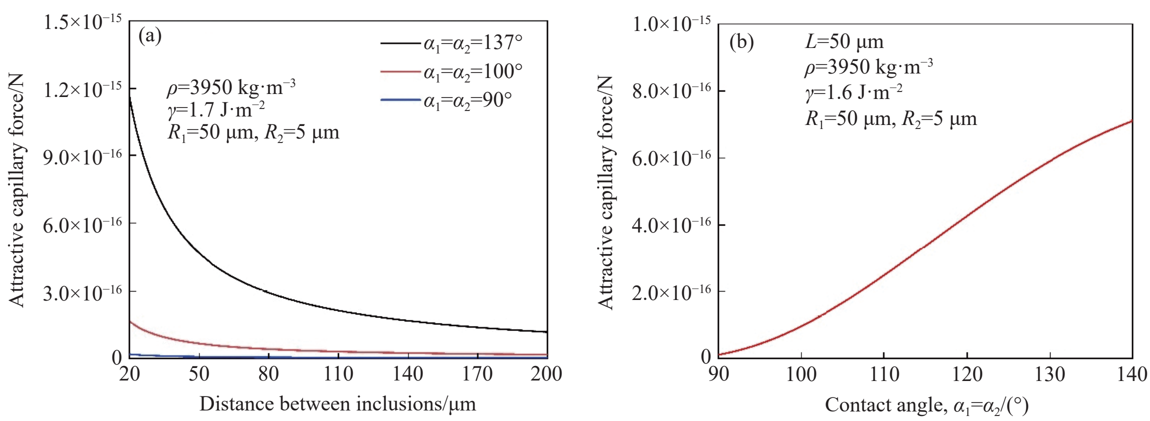

图 12 接触角与毛细吸力的关系. (a) 与钢液不同接触角夹杂物间毛细力随距离的变化; (b) 接触角与毛细力的关系[44]

Fig.12 Relationship between the contact angle and capillary force: (a) variation of capillary force with the distance between inclusions at different contact angles with molten steel; (b) the relationship between the contact angle and capillary force[44]

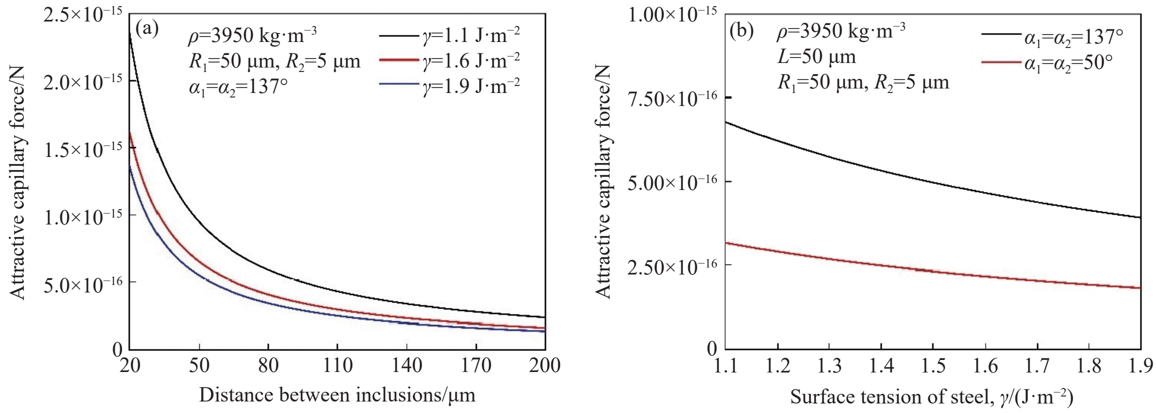

图 13　钢液表面张力与毛细力的关系. (a) 在不同钢液表面夹杂物间毛细吸力随距离的变化; (b) 表面张力与毛细力的关系[43]

Fig.13　Relationship between the surface tension and capillary force of molten steel: (a) variation of capillary force with the distance between inclusions on different surfaces of molten steel; (b) The relationship between surface tension and capillary force[43]

略有增加，无论夹杂物与钢液润湿与否，这一结论都是一致的，如图 13 (b) 所示. 由于钢液的表面张力受到不同钢种的影响，这一结论表明，如果润湿行为没有明显改变，各钢种的夹杂物团聚行为不会有明显的差异.

4　结论及展望

（1）高温共聚焦已经广泛应用于研究非金属夹杂物在钢/Ar 界面中的碰撞行为，对了解钢中非金属夹杂物的碰撞、团聚与长大行为及规律，探究提高钢洁净度的方法有重要意义；

（2）钢/Ar 界面夹杂物团聚的规律是：类似相的夹杂物对表现出吸引力，固相对表现出最强的吸引力，其次是半固–半固对和液–液对. 对于具有不同状态的夹杂物对，同时存在吸引力和排斥力. 这种差异取决于其物理性质，特别是夹杂物与钢液之间的接触角；

（3）对毛细管力模型的参数研究表明，夹杂物密度、尺寸和接触角对毛细吸力有显著的影响，钢液表面张力对毛细吸力的影响相对更弱；

（4）已有研究包含 Al_2O_3, Al_2O_3–SiO_2, Al_2O_3–CaO, MgO, Al_2O_3–MgO, Al_2O_3–Ce_2O_3 及碳钢中 Ca、Si、Al 类夹杂物，但对其他类复合夹杂物如 Ti 类氧化物、钛铝尖晶石等夹杂物的研究较少，同种元素不同梯度对夹杂物之间碰撞的影响也值得重点研究；

（5）计算钢/Ar 界面夹杂物之间毛细力 K–P 模型仍有较多不足，所需的物理性质数据较多，如各类夹杂物与钢液之间的接触角，难以计算钢液表面所有夹杂物之间毛细力大小，修正 K–P 模型或建立新的钢液表面夹杂物碰撞模型对研究钢液表面夹杂物碰撞趋势有着重要意义.

参　考　文　献

[1]　Zhang L F, Thomas B G. State of the art in evaluation and control of steel cleanliness. *ISIJ Int*, 2003, 43(3): 271

[2]　Zhang L F, Thomas B G. State of the art in the control of inclusions during steel ingot casting. *Metall Mater Trans B*, 2006, 37(5): 733

[3]　Wang C, Wang H, Zhang C, et al. A review on high temperature confocal scanning laser microscope applied in steel materials. *Phys Exam Test*, 2019, 37(6): 15
（王昌, 王辉, 张超, 等. 高温激光共聚焦显微镜在钢铁材料中研究进展. 物理测试, 2019, 37(6): 15）

[4]　Yin H B, Shibata H, Emi T, et al. Characteristics of agglomeration of various inclusion particles on molten steel surface. *ISIJ Int*, 1997, 37(10): 946

[5]　Yin H B, Shibata H, Emi T, et al. “In-situ” observation of collision, agglomeration and cluster formation of alumina inclusion particles on steel melts. *ISIJ Int*, 1997, 37(10): 936

[6]　Wang X X, Huang Q S. Acquiring high density of ultrafine second-phase nanoparticles quickly in low-carbon steel. *Chin J Eng*, 2024, 46(11): 2010
（王肖肖, 黄青松. 低碳钢中高密度超细纳米第二相粒子的快速获取. 工程科学学报, 2024, 46(11): 2010）

[7]　Wang J J, Zhang L F, Ren Y. Advances in the thermodynamics and kinetics of the steelmaking process and their application in numerical simulation. *Chin J Eng*, 2024, 46(11): 1960
（王举金, 张立峰, 任英. 炼钢过程反应热力学与动力学及其在数值模拟仿真的应用研究进展. 工程科学学报, 2024, 46(11): 1960）

[8]　Liu J J, Li J H, Li P H. Full-furnace pouring technology of long-life blast furnace lining integration. *Hebei Metall*, 2024(3): 82
（刘静静, 李京华, 李鹏辉. 长寿高炉炉衬一体化全炉浇注技术. 河北冶金, 2024(3): 82）

[9]　Lian H C, Lv B, Wang S G, et al. Preparation of green filling cementitious materials with low quality solid waste. *Hebei Metall*, 2024(3): 71

(连欢超, 吕波, 王社光, 等. 低品质固废协同制备绿色充填胶凝材料. 河北冶金, 2024(3): 71)

[10] Li X, Jin S R, Wang P F, et al. Research status and perspectives for cold rolling flatness control technology. *China Metall*, 2024, 34(7): 21
(李旭, 金树仁, 王鹏飞, 等. 冷轧板形控制技术的研究现状及展望. 中国冶金, 2024, 34(7): 21)

[11] Li M, Liu H B, Che X R, et al. Microsegregation models of solute elements during the solidification of high-carbon, medium-magnetic wear-resistant steel. *Chin J Eng*, 2024, 46(6): 1089
(李民, 刘洪波, 车晓锐, 等. 高碳中锰耐磨钢凝固过程溶质微观偏析模型. 工程科学学报, 2024, 46(6): 1089)

[12] Li D H, Duan H J, Sun L, et al. Effect of tundish structure optimization on flow state of molten steel. *China Metall*, 2024, 34(8): 38
(李顶涵, 段豪剑, 孙亮, 等. 中间包结构优化对钢液流动状态的影响. 中国冶金, 2024, 34(8): 38)

[13] Duan Y Q, Guo L, Zhang S, et al. Numerical simulation study on the floating of inclusions of different shapes in steel in a supergravity field. *Chin J Eng*, 2024, 46(5): 812
(段禹奇, 郭磊, 张帅, 等. 钢中不同形状夹杂物在超重力场中上浮模拟研究. 工程科学学报, 2024, 46(5): 812)

[14] Wang J, Peng J, Zhang F, et al. Thermodynamic calculation and experimental analysis on effects of rare earth Ce on TiN phase precipitation in 20CrMnTi steel. *Iron Steel*, 2024, 59(4): 66
(王健, 彭军, 张芳, 等. 稀土铈对 20CrMnTi 钢中 TiN 相析出热力学计算及分析. 钢铁, 2024, 59(4): 66)

[15] Li C X, Yao X, Lin Y, et al. Research progress in numerical simulation of waste heat recovery from blast furnace slag. *Iron Steel*, 2024, 59(5): 12
(李晨晓, 姚鑫, 林岩, 等. 高炉渣余热回收数值模拟研究进展. 钢铁, 2024, 59(5): 12)

[16] Coletti B, Blanpain B, Vantilt S, et al. Observation of calcium aluminate inclusions at interfaces between Ca-treated, Al-killed steels and slags. *Metall Mater Trans B*, 2003, 34(5): 533

[17] Liu J, Guo M, Jones P T, et al. *In situ* observation of the direct and indirect dissolution of MgO particles in $CaO–Al_2O_3–SiO_2$-based slags. *J Eur Ceram Soc*, 2007, 27(4): 1961

[18] Miao K Y, Haas A, Sharma M, et al. *In situ* observation of calcium aluminate inclusions dissolution into steelmaking slag. *Metall Mater Trans B*, 2018, 49(4): 1612

[19] Michelic S K, Dieguez Salgado U, Bernhard C. *In-situ* observation of the behaviour of non-metallic inclusions at different interfaces in the system steel-slag-refractory. *IOP Conf Ser: Mater Sci Eng*, 2016, 143: 012010

[20] Mu W Z, Dogan N, Coley K S. *In situ* observations of agglomeration of non-metallic inclusions at steel/Ar and steel/slag interfaces by high-temperature confocal laser scanning microscope: A review. *JOM*, 2018, 70(7): 1199

[21] Park J H, Kim D S. Effect of $CaO–Al_2O_3–MgO$ slags on the formation of $MgO–Al_2O_3$ inclusions in ferritic stainless steel. *Metall Mater Trans B*, 2005, 36(4): 495

[22] Wu M H, Ren C Y, Ren Y, et al. *In situ* observation of the agglomeration of $MgO–Al_2O_3$ inclusions on the surface of a molten GCr15-bearing steel. *Metall Mater Trans B*, 2023, 54(3): 1159

[23] Shibata H, Yin H, Emi T. The capillary effect promoting collision and agglomeration of inclusion particles at the inert gas–steel interface. *Philos Trans R Soc Lond Ser A Math Phys Eng Sci*, 1998, 356(1739): 957

[24] Liang G F, Wang C Q, Fang Y. *In situ* observation on movement and agglomeration of inclusion in solid liquid mush zone during melting of stainless steel aisi304. *Acta Metall Sin*, 2006, 42(7): 708
(梁高飞, 王成全, 方园. AISI304 不锈钢熔化过程中夹杂物在固–液糊状区漂移与聚集行为的原位观察. 金属学报, 2006, 42(7): 708)

[25] Kimura S, Nakajima K, Mizoguchi S. Behavior of alumina-magnesia complex inclusions and magnesia inclusions on the surface of molten low-carbon steels. *Metall Mater Trans B*, 2001, 32(1): 79

[26] Kimura S, Nabeshima Y, Nakajima K, et al. Behavior of nonmetallic inclusions in front of the solid-liquid interface in low-carbon steels. *Metall Mater Trans B*, 2000, 31(5): 1013

[27] Nakajima K, Mizoguchi S. Capillary interaction between inclusion particles on the 16Cr stainless steel melt surface. *Metall Mater Trans B*, 2001, 32(4): 629

[28] Wikström J, Nakajima K, Shibata H, et al. *In situ* studies of the agglomeration phenomena for calcium–alumina inclusions at liquid steel–liquid slag interface and in the slag. *Mater Sci Eng A*, 2008, 495(1–2): 316

[29] Wikström J, Nakajima K, Shibata H, et al. *In situ* studies of agglomeration between Al_2O_3–CaO inclusions at metal/gas, metal/slag interfaces and in slag. *Ironmak Steelmak*, 2008, 35(8): 589

[30] Lee S H, Tse C, Yi K W, et al. Separation and dissolution of Al_2O_3 inclusions at slag/metal interfaces. *J Non Cryst Solids*, 2001, 282(1): 41

[31] Khurana B, Spooner S, Rao M B V, et al. *In situ* observation of calcium oxide treatment of inclusions in molten steel by confocal microscopy. *Metall Mater Trans B*, 2017, 48(3): 1409

[32] Appelberg J, Nakajima K, Shibata H, et al. *In situ* studies of misch-metal particle behavior on a molten stainless steel surface. *Mater Sci Eng A*, 2008, 495(1-2): 330

[33] Wang Y G, Liu C J. Agglomeration characteristics of various inclusions in Al-killed molten steel containing rare earth element. *Metall Mater Trans B*, 2020, 51(6): 2585

[34] Bin W, Bo S. *In situ* observation of the evolution of intragranular acicular ferrite at Ce-containing inclusions in 16Mn steel. *Steel Res Int*, 2012, 83(5): 487

[35] Wang Y G, Liu C J. Agglomeration characteristics of various oxide inclusions in molten steel containing rare earth element

under different deoxidation conditions. *ISIJ Int*, 2021, 61(5): 1396

[36] Tian Q R, Wang G C, Shang D L, et al. *In situ* observation of the precipitation, aggregation, and dissolution behaviors of TiN inclusion on the surface of liquid GCr15 bearing steel. *Metall Mater Trans B*, 2018, 49(6): 3137

[37] Misra P, Sridhar S, Cramb A W. *In-situ* observation of TiN precipitates at stainless steel/CaO–Al_2O_3–MgO–SiO_2 interface. *Metall Mater Trans B*, 2001, 32(5): 963

[38] Misra P, Chevrier V, Sridhar S, et al. *In situ* observations of inclusions at the (Mn, Si) -killed steel/CaO–Al_2O_3 interface. *Metall Mater Trans B*, 2000, 31(5): 1135

[39] Shao X, Wang X, Jiang M, et al. *In Situ* observation of mns inclusion behavior in resultfurized free-cuttinig steel during heating. *Acta Metall Sin*, 2011, 47(9): 1210

[40] Yan P C, Guo M X, Blanpain B. *In situ* observation of the formation and interaction behavior of the oxide/oxysulfide inclusions on a liquid iron surface. *Metall Mater Trans B*, 2014, 45(3): 903

[41] Aneziris C G, Schroeder C, Emmel M, et al. *In situ* observation of collision between exogenous and endogenous inclusions on steel melts for active steel filtration. *Metall Mater Trans B*, 2013, 44(4): 954

[42] Vantilt S, Coletti B, Blanpain B, et al. Observation of inclusions in manganese-silicon killed steels at steel-gas and steel-slag interfaces. *ISIJ Int*, 2004, 44(1): 1

[43] Mu W Z, Dogan N, Coley K S. Agglomeration of non-metallic inclusions at steel/Ar interface: *in situ* observation experiments and model validation. *Metall Mater Trans B*, 2017, 48(5): 2379

[44] Mu W Z, Dogan N, Coley K S. Agglomeration of non-metallic inclusions at the steel/Ar interface: Model application. *Metall Mater Trans B*, 2017, 48(4): 2092

[45] Mu W Z, Dogan N, Coley K S. *In situ* observation of deformation behavior of chain aggregate inclusions: A case study for Al_2O_3 at a liquid steel/argon interface. *J Mater Sci*, 2018, 53(18): 13203

[46] Chen R, Chen Z P, Xu Y T, et al. *In-situ* observation of behaviors of inclusions in bearing steel. *J Iron Steel Res*, 2015, 27(12): 48
(陈然, 陈兆平, 徐迎铁, 等. 轴承钢夹杂物行为的原位观察. 钢铁研究学报, 2015, 27(12)：48)

[47] Jiang M, Wang X H, Pak J J, et al. *In situ* observation on behaviors of CaO–MgO–Al_2O_3–SiO_2 complex inclusions at solid–liquid interface of low-oxygen special steel. *Metall Mater Trans B*, 2014, 45(5): 1656

[48] Kang Y, Sahebkar B, Scheller P R, et al. Observation on physical growth of nonmetallic inclusion in liquid steel during ladle treatment. *Metall Mater Trans B*, 2011, 42(3): 522

[49] Mu H Y, Zhang T S, Yang L, et al. *In situ* observation of MgO inclusions in liquid iron-aluminum alloys. *Metall Mater Trans B*, 2016, 47(6): 3375

[50] Mu W Z, Xuan C J. Agglomeration mechanism of complex Ti–Al oxides in liquid ferrous alloys considering high-temperature interfacial phenomenon. *Metall Mater Trans B*, 2019, 50(6): 2694

[51] Wu M H, Ren Y, Zhang L F. *In-situ* observation of collision and agglomeration of La_2O_3–La_2S_3 inclusions on surface of molten 304 stainless steels. *Metall Mater Trans B*, 2024, 55(4): 2324

[52] Shibata H, Yin H B, Yoshinag S, et al. *In-situ* observation of engulfment and pushing of nonmetallic inclusions in steel melt by advancing melt/solid lnterface. *ISIJ Int*, 1998, 38(2): 149

[53] Du G, Li J, Wang Z B, et al. Effect of magnesium addition on behavior of collision and agglomeration between solid inclusion particles on H13 steel melts. *Steel Res Int*, 2017, 88(3): 1600185

[54] Cheng L M, Zhang L F, Shen P. Fundamentals of interfacial wettability in ironmaking and steelmaking. *Chin J Eng*, 2018, 40(12): 1434
(程礼梅, 张立峰, 沈平. 钢铁冶金过程中的界面润湿性的基础. 工程科学学报, 2018, 40(12)：1434)

[55] Qiu Z L, Malfliet A, Blanpain B, et al. Capillary interaction between arbitrarily-shaped inclusions at the gas/steel interface. *Metall Mater Trans B*, 2022, 53(3): 1894

[56] Qiu Z L, Malfliet A, Blanpain B, et al. Capillary interaction between micron-sized Ce_2O_3 inclusions at the Ar gas/liquid steel interface. *Metall Mater Trans B*, 2022, 53(3): 1775

[57] Paunov V N, Kralchevsky P A, Denkov N D, et al. Lateral capillary forces between floating submillimeter particles. *J Colloid Interface Sci*, 1993, 157(1): 100

[58] Kralchevsky P A, Nagayama K. Capillary interactions between particles bound to interfaces, liquid films and biomembranes. *Adv Colloid Interface Sci*, 2000, 85(2-3): 145